COMMUNICATIONS PHYSICS

ARTICLE

https://doi.org/10.1038/s42005-020-00516-w OPEN

Amplitude death and restoration in networks of oscillators with random-walk diffusion

Pau Clusella [1✉], M. Carmen Miguel[2,3] & Romualdo Pastor-Satorras [1]

Systems composed of reactive particles diffusing in a network display emergent dynamics. While Fick's diffusion can lead to Turing patterns, other diffusion schemes might display more complex phenomena. Here we study the death and restoration of collective oscillations in networks of oscillators coupled by random-walk diffusion, which modifies both the original unstable fixed point and the stable limit-cycle, making them topology-dependent. By means of numerical simulations we show that, in some cases, the diffusion-induced heterogeneity stabilizes the initially unstable fixed point via a Hopf bifurcation. Further increasing the coupling strength can moreover restore the oscillations. A numerical stability analysis indicates that this phenomenology corresponds to a case of amplitude death, where the inhomogeneous stabilized solution arises from the interplay of random walk diffusion and heterogeneous topology. Our results are relevant in the fields of epidemic spreading or ecological dispersion, where random walk diffusion is more prevalent.

[1] Departament de Física, Universitat Politècnica de Catalunya, Campus Nord B4, 08034 Barcelona, Spain. [2] Departament de Física de la Matèria Condensada, Universitat de Barcelona, Martí i Franquès 1, 08028 Barcelona, Spain. [3] Universitat de Barcelona Institute of Complex Systems (UBICS), Universitat de Barcelona, Martí i Franquès 1, 08028 Barcelona, Spain. ✉email: pau.clusella@upc.edu

Complex systems composed by many units interrelated through a heterogeneous topological pattern of interactions form a wide class of natural and man-made systems that can be fruitfully represented in terms of complex networks[1]. Under this representation, in which nodes stand for units and edges for pairwise unit interactions, a natural framework arises that is capable of unifying the functional and structural properties of a wide variety of different systems. Particularly important in this respect are those systems that are the substrate for some dynamic of transport process, whose properties can be strongly impacted by the topology of interaction[2,3].

A versatile formalism to describe dynamical processes on networks is given by the theory of reaction–diffusion processes, described in terms of different kinds of particles or species that diffuse along the edges of the network and interact among them inside the nodes. Reaction–diffusion systems find a natural representation in terms of sets of nonlinear differential equations, representing in-node interactions, coupled by a diffusion term representing transport between nodes. Successful applications of this formalism can be found, for example, in the study of ecological species dispersal[4] or epidemic spreading[5]. In these studies, the network structure represents a metapopulation[6], defined as a group of populations or physical patches, joined by migration or mobility paths.

In the context of reaction–diffusion systems on networks, it is particularly noteworthy the work of Nakao and Mikhailov[7], where it was outlined the relation between the usual understanding of pattern formation in reaction–diffusion systems in lattices, established by the seminal work of Turing[8], and its counterpart in irregular topologies. In both cases, the stability of the homogeneous equilibrium, preserved by the diffusion, can be attained by means of the dispersion relation, which, in the complex network case, relies on the diagonalization of a Laplacian operator[7,9,10]. As a result, Turing patterns are observed to arise in networked substrates, characterized by a node-dependent pattern of species density[7]. The observation of Nakao and Mikhailov has spurred a flurry of activity in the field of reaction–diffusion processes on networks, leading to the study of the effects of directedness in the network edges[10], the competition in predator-prey models[11], the effects on limit cycles[12], the role of time-varying networks[13], and methods for pattern tunning[14–16].

Most previous works, however, are based on models where the coupling follows Fick's diffusion law, used to model chemical reactions and heat transport. In this case, the exchange rate of the physical quantities between two nodes is proportional to their density difference. A different choice for the diffusive coupling that can be considered on complex networks corresponds to random-walk diffusion[5,17,18]. In this case the exchange rate between two nodes is proportional to the inverse of their degree, thus corresponding to particles diffusing by jumping between randomly chosen nearest neighbor sites. This version of diffusion is particularly relevant in the case of ecology dynamics where each node represents a population of a certain species in an ecosystem, which then might randomly migrate to the surrounding environments[19,20]. Random walks have been extensively studied in complex networks[21], but their application in the context of reaction–diffusion systems is rather limited[5,17,18,22].

The differences between the two coupling schemes significantly affect the nature of the system. As a starting point, except for specifically devised cases[23], random-walk diffusion does not accept, in general, a homogeneous equilibrium, hence the steady states are topology-dependent[17]. As direct implication of this situation, even if an equilibrium point of the network is known, its stability will depend on both its shape and the underlying Laplacian, thus making an analytical treatment in terms of a dispersion relation difficult. In fact, most of the existing literature on the topic addresses the question of how random-walk diffusion modifies the steady states of the system[5,17,18], the manifestation of Turing bifurcations using random-walk diffusion[17], and how such inhomogeneous states might be used to identify topological properties of the underlying network[22].

Oscillatory systems represent an important class for the choice of the reaction terms. Complex oscillatory systems are indeed used as a proxy to study many relevant phenomena such as chemical reactions[24,25], cardiac cells[26,27] neural dynamics[28,29], and ecological fluctuations[30,31]. Amplitude Death and Oscillation Death are the two main routes through which the coupling among the oscillatory units leads to a state of steadiness[32]. Although the two mechanisms have been prone to confusion, they correspond to two different dynamical phenomena, with different implications on their applicability. The emergence of OD occurs when the coupling among units induces the creation of new inhomogeneous stationary solutions. Upon modifying the coupling strength, an originally oscillatory solution, such as a limit-cycle, is destabilized and the system falls into the steady state created by the coupling. Nevertheless, the (unstable) oscillatory solution and the inhomogeneous fixed-point coexist[12,25]. On the other hand, AD occurs when different coupled oscillators pull each other out of the limit-cycle upon increasing the interaction strength. Thus, the amplitude of the oscillations diminish until it completely vanishes and the oscillators fall into the homogeneous fixed point of the system. Therefore, in this case, the oscillatory solution collapses into the steady state and there is no coexistence[33–35].

In oscillatory systems coupled with Fick's diffusion it is possible to compute the dispersion relation associated to the homogeneous time-varying solution, whose instability leads to Turing patterns. If these patterns are steady in time, then we are before a case of OD[12]. Nevertheless, as we review in detail in this paper, the AD phenomena is forbidden in networks with identical reaction terms and Fick's diffusion, as the instability of the homogeneous fixed point is preserved by the coupling[33]. Therefore, one needs to invoke further complexity on the description of the model, such as distributed frequencies[34], delayed interactions[35], or dynamic coupling[36]. Choosing random-walk diffusion strongly modifies this scenario.

In this paper, we show a novel instance, to the best of our knowledge, of emerging collective behavior induced by random-walk diffusion beyond the Turing paradigm. In particular, we investigate a phenomena which is forbidden in reaction systems with Fick's diffusion: the quenching of the oscillatory dynamics through the Amplitude Death mechanism, as opposed to the Oscillation Death mechanism that has been indeed studied in systems with Fick's diffusion[32]. Here, we show that an increase of the diffusion strength diminishes the amplitude of the oscillations until they collapse into an inhomogeneous steady state. This phenomena differs from OD in the sense that there is no coexistence between the oscillatory solution and the fixed point. We show that the stationary solution corresponds to the uncoupled local equilibria of each node that has been modified anisotropically by the coupling. Therefore, the cease of the oscillations corresponds a case of AD where the stabilized solution is inhomogeneous. Here we extensively study this transition towards AD and the later restoration of the oscillations, as well as we show how suitable modifications of the network topology lead towards the disappearance of AD. We also perform heterogeneous mean-field analysis in order to validate the generality of this phenomena for large systems.

Results and discussion

Gradient-driven diffusion. In this section, we illustrate how Fick's diffusion law affects oscillatory solutions in reaction–diffusion

systems. In particular, we show that OD phenomena might emerge as a Turing bifurcation of the limit-cycle solution, whereas AD is not possible in such setup.

General two-species reaction–diffusion processes on a network can be represented by the set of equations

$$\begin{cases} \dot{x}_i = & f(x_i, y_i) + D_x \sum_{j=1}^{N} \Delta_{ij} x_j \\ \dot{y}_i = & g(x_i, y_i) + D_y \sum_{j=1}^{N} \Delta_{ij} y_j \end{cases},$$

where D_x and D_y are the coupling (diffusion) coefficients, f and g are nonlinear reactive terms, and the matrix Δ_{ij} is the discrete Laplacian operator specifying the diffusive transport of species between connected nodes. If diffusive transport is ruled by Fick's law, that is, by the sum of fluxes of incoming species at each node, where the flux is assumed to be proportional to the concentration[37], the discrete Laplacian can be written as $\Delta_{ij} = a_{ij} - k_i\delta_{ij}$, where k_i is the degree of node i, δ_{ij} is the Kronecker symbol and a_{ij} is the network adjacency matrix, taking value 1 when nodes i and j are connected, and zero otherwise[1]. In this case the equations of motion ruling the dynamics of the ith node of the network read

$$\begin{cases} \dot{x}_i = & f(x_i, y_i) + D_x \sum_{j=1}^{N} a_{ij}(x_j - x_i) \\ \dot{y}_i = & g(x_i, y_i) + D_y \sum_{j=1}^{N} a_{ij}(y_j - y_i) \end{cases}. \quad (1)$$

For this gradient-driven diffusion scheme, any solution of the uncoupled system ($D_x = D_y = 0$) corresponds to a solution of the coupled system. Indeed, the diffusion term only depends on the density difference between connected nodes, so if all nodes evolve with the exact same dynamics, $(x_j(t), y_j(t)) = (x(t), y(t))$ for all $j = 1, \ldots, N$, then the diffusive coupling vanishes and the solution is preserved. Such solutions are homogeneous, meaning that the dynamical evolution of the system is the same for all nodes independently of their topological properties. As we consider that the dynamics of each node has two dimensions, only two types of attractors are possible here: (i) fixed points of the original uncoupled system, $(x^{(0)}, y^{(0)})$, and (ii) periodic solutions, also referred to as limit cycles[38].

The addition of the coupling diffusive terms can spontaneously modify the stability of these homogeneous solutions. In principle, the stability of a homogeneous fixed point of system (1) boils down to study the eigenvalues λ_i of a $2N \times 2N$ Jacobian matrix. Nevertheless, it is possible to relate the eigenvalues of such high-dimensional operator to the eigenvalues of the Laplacian matrix of the system by means of a dispersion relation

$$\lambda = F(\Lambda)$$

which maps all the Laplacian matrix eigenvalues Λ_j to the eigenvalues of the system Jacobian λ_j. This corresponds to the extension of discrete dispersion relations in lattices to the complex network case[7,39] (see Methods for a detailed explanation). We notice that other works define the dispersion relation in terms of the largest real part of λ.

In order to illustrate this situation, we consider as an example the Brusselator model, whose dispersion relation can be worked out analytically (see Methods). As it is well-known, if the network has a single connected component, the associated Laplacian always contains a single zero eigenvalue corresponding to a uniform eigenvector, and the rest are all negative. In the dispersion relation, such zero eigenvalue always returns the eigenvalues of the uncoupled Jacobian (see Eq. (9) in Methods). Assuming that the fixed point is originally stable for $D_x = D_y = 0$, the rest of the eigenvalues associated to the strictly negative Laplacian eigenmodes might have a positive real part, thus destabilizing the homogeneous solution and generating spatio-temporal patterns. This is the well-known Turing instability, which triggers the so-called Turing patterns[7,8,39].

Instead, here we are interested in oscillatory systems, thus, we set the system parameters as $a = 1.3$ and $b = 2.5$ so that the fixed point of the uncoupled system is unstable and the Brusselator displays periodic motion. The resulting dispersion relation is depicted in Fig. 1a, where we plot the real part of the eigenvalues controlling the stability of $(x^0, y^{(0)})$ as a function of the eigenvalues of the Laplacian Λ_j for the case of an homogeneous Erdös-Rényi (ER) network (see Methods). In this case, the system eigenvalue corresponding to the uniform eigenvector, which is associated to the zero Laplacian eigenvalue, has $\mathrm{Re}[\lambda_0] = 0.1$. In other words, Fick's diffusion law preserves the unstability of the homogeneous fixed-point and, therefore, the AD phenomena, in which the focus of a limit-cycle is stabilized through the coupling, cannot manifest here.

On the other hand, performing a stability analysis of the limit-cycle solution shows that the periodic solution might be distabilized through a Turing mechanism, thus potentially leading to a case OD. Indeed, it is possible to derive a numerical (and, in some cases, analytical), dispersion relation of the Floquet exponents corresponding to the homogeneous limit-cycle by means of the master stability function[9,12]. Figure 1b depicts the relation between the Floquet exponents μ_j of the limit-cycle for

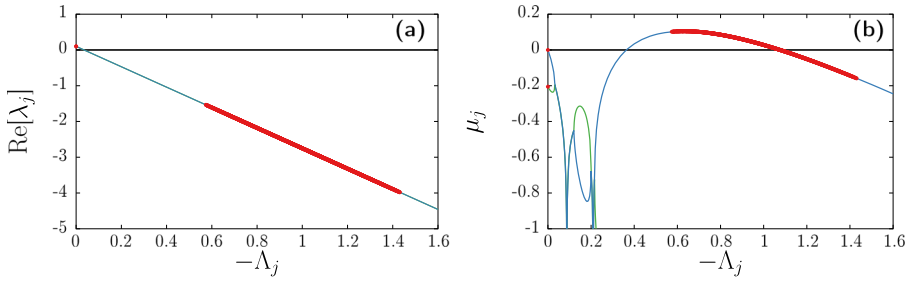

Fig. 1 Dispersion relation for the Brusselator system with Fick's diffusion. Red dots indicate the discrete dispersion relation as obtained by diagonalizing the Laplacian operator (see Methods) corresponding to an Erdös-Rényi network with $N = 1000$ nodes and average degree $\langle k \rangle = 20$. Continuous lines show the continuous dispersion relation associated to a lattice at the thermodynamic limit (see Methods). System parameters of the reactive terms are $a = 1.3$ and $b = 2.5$. Diffusion values are $D_x = 0.7$ and $D_y = 5$. **a** Real part of the eigenvalues λ_j controlling the stability of the homogeneous fixed point as a function of the Laplacian eigenvalues Λ_j, $j = 1, ..., 2N$. **b** Real part of the Floquet exponents μ_j controlling the stability of the homogeneous limit-cycle solution as a function of the Laplacian eigenvalues Λ_j, $j = 1, ..., 2N$. Since we are considering two-dimensional single-node dynamics, blue and green continuous lines show the two different branches of the dispersion relation whenever they are different, such as in **b**. Notice that with our definition of the Laplacian, the eigenvalues Λ_j are non-positive, thus we display $-\Lambda_j$ in the x axis. Other works might use a different definition.

the Brusselator system and the eigenvalues of the network Laplacian. The Floquet exponents corresponding to the uniform eigenvector are $\mu_0^+ = 0$ and $\mu_0^- \simeq -0.216$, but there are many other Floquet exponents associated to different network Laplacian modes that are positive. Thus, in this case, the originally stable limit-cycle is being destabilized through a Turing instability, so an arbitrary perturbation of the homogeneous solution will develop heterogeneous patterns. If these heterogeneous patterns are stationary, then we would be before a case of OD[12].

Random-walk diffusion. Let us move now to a different coupling, the so-called random-walk diffusion[18,22]. Here variables x_j and y_j might represent the population density of animals that coexist in an ecosystem divided in different discrete patches (a metapopulation[6]). Animals interact inside patches following some nonlinear dynamics and can migrate between connected patches. Representing the pattern of connections between patches by a network, and assuming that animals move at random between patches, we have that population of node i diffuses uniformly through its k_i neighbors, each receiving a flux proportional to $1/k_i$. The Laplacian matrix can thus be written as $\tilde{\Delta} = (\tilde{\Delta}_{ij})$, with $\tilde{\Delta}_{ij} = a_{ij}/k_j - \delta_{ij}$. The reaction–diffusion process then reads

$$\begin{cases} \dot{x}_i = & f(x_i, y_i) + D_x \left(\sum_{j=1}^{N} a_{ij} \frac{x_j}{k_j} - x_i \right) \\ \dot{y}_i = & g(x_i, y_i) + D_y \left(\sum_{j=1}^{N} a_{ij} \frac{y_j}{k_j} - y_i \right) \end{cases} . \qquad (2)$$

Here, the solution of the uncoupled system ($D_x = D_y = 0$) is not a solution of the coupled system unless we have a regular network, i.e., all nodes have the same degree $k_i = k \, \forall \, i$. In this case, one can again study the stability of the system by means of a dispersion relation and the arguments exposed above still hold. However, for generic non-regular networks there is no theory that applies, and thus, the collective effects induced by the coupling are unknown.

To study the effects of random-walk diffusion, we consider the Brusselator dynamics and integrate numerically the system defined by Eq. (2) in an ER network with average degree $\langle k \rangle = 20$ (see Methods). For simplicity we set $D_x = D_y = D$ throughout the rest of the paper. Unequal diffusion coefficients can lead to much more complex dynamics; in fact, the generation of static Turing patterns in models with Fick's diffusion requires $D_x \neq D_y$ and, in particular, it requires than the inhibitor diffuses much faster than the activator, i.e., $D_y \gg D_x$ in our case[39,40]. Unless otherwise stated, we set the system parameters $a = 0.5$ and $b = 1.7$, thus an uncoupled oscillator displays oscillatory behavior (see Methods). In Fig. 2 we show the evolution of the variable y_i resulting from numerical integration for different values of the diffusion coefficient D and starting from random initial conditions uniformly distributed $x_j(0), y_j(0) \in [0.2, 0.8]$.

In Fig. 2a, we can see that a very small diffusion $D = 0.02$ does not strongly affect the behavior of the system. The limit cycle defined by the variables in each node oscillates with a very similar amplitude and period, this last one close to the estimate for an isolated Brusselator, $T = 2\pi/\sqrt{a}$. The different oscillators fluctuate however out-of-phase. Upon increasing the coupling, (Fig. 2b, corresponding to $D = 0.3$), the oscillators evolve in periodic phase-synchrony, but each having a different amplitude of the limit-cycle, amplitude that is related to the degree of the corresponding node in the network (see Supplementary Fig. 6a in Supplementary Note 2). Increasing the coupling to $D = 2$, (Fig. 2c), the system reaches a steady state, the heterogeneous oscillations being substituted by a heterogeneous fixed point, whose value is also related to the node's degree. Further

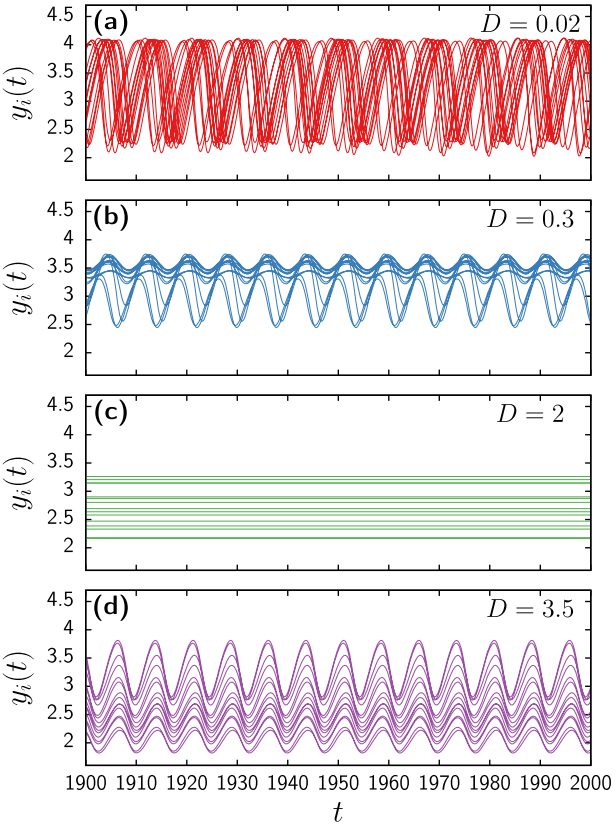

Fig. 2 Time series of individual nodes of the Brusselator system with random-walk diffusion. Each line indicates the time evolution of the y variable of node i, where i corresponds to 15 randomly chosen nodes (same nodes for each panel). Results obtained from the numerical integration of the Brusselator model Eq. (10) with random-walk diffusion Eq. (2) on an Erdös-Rényi networks of size $N = 1000$ and average degree $\langle k \rangle = 20$. System parameters for the Brusselator reaction terms are $a = 0.5$, $b = 1.7$. The values of diffusion coefficient are **a** $D = 0.02$, **b** $D = 0.3$, **c** $D = 2$, and **d** $D = 3.5$.

increasing of the coupling up to $D = 3.5$ (Fig. 2d), restores the in-phase synchrony, with node-dependent amplitude. These preliminary observations indicate the existence of an oscillation quenching phenomenon, and a later oscillation restoration. In the oscillatory regimes for $D > 0$, the nodes appear to have the same period (except in the vicinity of the first oscillation quenching transition), period that depends on D, as a power spectrum analysis reveals (see Supplementary Fig. 5a). Whether it corresponds to OD or AD is not yet clear.

In order to characterize the oscillation quenching behavior of the system we consider the average of variable y over the whole network,

$$\bar{y}(t) = \frac{1}{N} \sum_{j=1}^{N} y_j(t) \ ,$$

and measure the temporal average $\langle \bar{y} \rangle$ and standard deviation $\sigma = \sigma(\bar{y})$, defined as

$$\begin{aligned} \langle \bar{y} \rangle &= \lim_{T \to \infty} \frac{1}{T} \int_0^T \bar{y}(t') \, dt', \ \sigma(\bar{y})^2 \\ &= \lim_{T \to \infty} \frac{1}{T} \int_0^T \bar{y}(t')^2 \, dt' - \langle \bar{y} \rangle^2, \end{aligned} \qquad (3)$$

that works as a measure of the average amplitude of oscillations, with $\sigma = 0$ indicating a steady state.

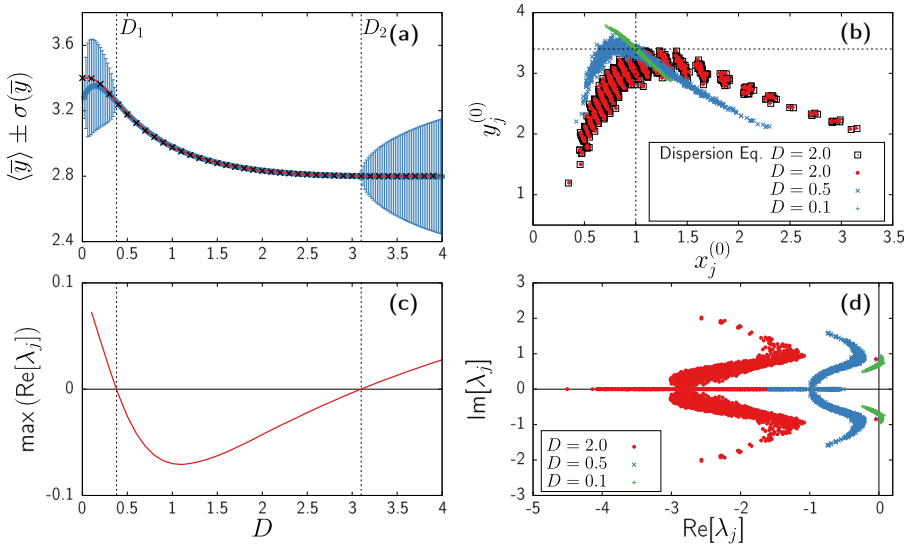

Fig. 3 Results of simulations and numerical analysis for the Brusselator model in an Erdös-Rényi (ER) network. System parameters for the reactive terms are $a = 0.5$ and $b = 1.7$. Network topology corresponding to a ER with $N = 1000$ nodes and average degree $\langle k \rangle = 20$. **a** Blue circles indicate the time-averaged mean-field corresponding to the y variable of each node, $\langle \bar{y} \rangle$, obtained from numerical simulations for different values of diffusion D. Error bars indicate the temporal standard deviation of the mean-field, $\sigma(\bar{y})$ (definitions in the text). Red continuous line shows the mean-field corresponding to the heterogeneous fixed point obtained solving numerically the system of equations (4). Black crosses correspond to the mean-field obtained by integrating the peturvative equation (5). Vertical black dashed lines indicate the bifurcation points derived from the stability analysis. **b** Coordinates of the heterogeneous fixed point of the system $(x_j^{(0)}, y_j^{(0)})$, $j = 1, ..., N$, in the phase space. Green plusses, blue crosses, and red points correspond to numerical solutions of system (4) for different diffusion values D. Black squares correspond to the solution obtained by integrating Eq. (5) up to $D = 2$. Each symbol corresponds to a different network node $j = 1, ..., N$. The crossing of the two black dashed lines indicate the equilibria of the uncoupled system, $(x^{(0)}, y^{(0)}) = (1, b/a)$. **c** Largest eigenvalue's real part for different values of D. Vertical black dashed lines indicate the bifurcation points where the largest eigenvalue crosses de x axis. **d** Eigenvalue spectra in the complex plane for different values of D (same symbols as in **b**).

In Fig. 3a we show in blue circles the value of $\langle y \rangle$ as a function of the diffusion coefficient D. The associated error bars indicate the corresponding standard deviation $\sigma(\bar{y})$. For small values of D the network displays oscillatory dynamics, as indicated by the non-zero amplitude $\sigma(\bar{y})$. Upon increasing D, such oscillations diminish until they vanish completely for diffusion larger than $D_1 \simeq 0.3775$. The system is frozen in a heterogeneous steady state until the oscillations are restored again for a diffusion D larger than $D_2 \simeq 3.095$. We are therefore in front of a case of oscillation quenching occurring at D_1, followed by a subsequent oscillation restoration when D crosses D_2. Whereas the inhomogeneity of the fixed point would support the idea that the phenomenology corresponds to OD, the two transitions between oscillatory and steady regimes strongly resemble the AD phenomena, where the periodic solutions collapse into the fixed point, which in this case happens to be heterogeneous as opposed to the common cases of AD[32,41]. In the following, we study the two bifurcations through which the oscillations vanish and restore in order to unveil the mechanism responsible for the cessation of the oscillations.

Heterogeneous fixed points. In order to investigate the nature of these transitions, we start considering the underlying fixed points, corresponding to the solutions of the nonlinear system

$$\begin{cases} f(x_i, y_i) + D\sum_{j=1}^{N} \tilde{\Delta}_{ij} x_j = 0, \\ g(x_i, y_i) + D\sum_{j=1}^{N} \tilde{\Delta}_{ij} y_j = 0\ , \end{cases} \tag{4}$$

that we solve numerically using a standard multidimensional root solver based on the Newton-Raphson method[42]. Figure 3b shows the results obtained for different values of D in the phase space. For any value of $D > 0$, we obtain an inhomogeneous solution, i.e., depending on the node i, that for small values of D is relatively close to the fixed point of the uncoupled system ($x^{(0)} = 1, y^{(0)} = b/a$) (see green points). Upon increasing D, the network equilibria spread, covering a wider area of the phase space. For large diffusion (see for instance red dots, corresponding to $D = 2$) the solution shows clusters of nodes with similar values which correspond to nodes with the same degree (see Supplementary Fig. 6b). In principle nothing prevents the existence of other solutions. Nevertheless, it is worth noticing that we find only one solution of Eq. (4) for each value of D. Overall, it looks like the random-walk diffusion induces the hetoregeneity of the equilibria, which becomes homogeneous only for $D = 0$. The analysis presented in the next section provides a more rigorous analysis of this situation via a perturbative approach.

Dispersion of the fixed point. The previous numerical analysis points out that the heterogeneous equilibrium of the network is linked with the equilibrium of the uncoupled system for small diffusion values, thus indicating that the fixed point of the network corresponds to a coupling induced modification of the original steady state. We validate this assumption by exploring the effect that small modifications of the coupling strength D have on the fixed point. Let $(x_j^{(0)}(D), y_j^{(0)}(D))$ be the solution of Eqs. (4) for the diffusion value D. Assuming that the dependence on D is smooth, we consider a small increment of the diffusion, $\epsilon > 0$. Expanding up to first-order terms in equation (4) one obtains (see Methods for a detailed derivation) the system of equations

$$J\left(x_i^{(0)}, y_i^{(0)}\right)\begin{pmatrix} \frac{dx_i^{(0)}}{dD} \\ \frac{dy_i^{(0)}}{dD} \end{pmatrix} + D\sum_{j=1}^{N} \tilde{\Delta}_{ij}\begin{pmatrix} \frac{dx_j^{(0)}}{dD} \\ \frac{dy_j^{(0)}}{dD} \end{pmatrix} = -\sum_{j=1}^{N} \tilde{\Delta}_{ij}\begin{pmatrix} x_j^{(0)} \\ y_j^{(0)} \end{pmatrix} \tag{5}$$

for $i = 1, \ldots, N$, where $J(x, y)$ is the 2×2 Jacobian matrix of the (uncoupled) reactive field, $(f(x, y), g(x, y))$. Such equations form an implicit linear non-autonomous system of differential equations with the diffusion strength D as an independent variable.

An analytical solution of system in Eq. (5) is generally unfeasible, but a simple numerical integration of such equation using Euler's method, starting from the uncoupled system equilibrium, leads to the average activity reported in black crosses in Fig. 3a, whereas black squares in Fig. 3b correspond to the fixed point obtained with this method for $D = 2$. Both results match the solutions obtained by directly solving Eqs. (4), hence confirming that the heterogeneous equilibria of the system coupled through random-walk diffusion corresponds to a modification of the solution of the uncoupled system. In other words, the steady state is not a completely new state induced by the coupling, but a smooth transformation of the original equilibrium of the system, which turns out to be node-dependent as soon as $D > 0$. As the steady state associated with OD corresponds to new states created by the coupling, the observation that here the fixed point is not new is key to classify the observed oscillation quenching mechanism as AD rather than OD.

Stability analysis. With the numerical solution of the system obtained by directly solving Eq. (4) one can study the stability of the system by numerically computing the eigenvalues and eigenvectors of the full system $2N \times 2N$ Jacobian using standard numerical tools[42]. Figure 3c shows the dependence of the real part of the maximum eigenvalue as the diffusion D is tuned and Fig. 3d shows the full spectra for three different values of the diffusion. As it happens with the fixed point, for small D all the eigenvalues are located close to the eigenvalues of the uncoupled system $\lambda_{\pm} = 0.1 \pm 0.7i$. Thus, there is at least a pair of complex conjugate eigenvalues with positive real part. As D increases, most of the eigenvalues rapidly spread and are pushed to the left of the complex plane. Nevertheless, a pair of complex conjugate eigenvalues remain isolated from the rest and do not cross the imaginary axis until D_1 (see isolated symbols close to the imaginary axis in fig. 3d). Upon further increasing the diffusion, the same isolated pair of eigenvalues crosses again the imaginary axis at D_2, signaling the restoration of the oscillations (see Fig. 3c). According to these results, it is clear that both transitions, D_1 and D_2, are Hopf supercritical bifurcations. Indeed, as shown in Fig. 4, the amplitude of the oscillations vanishes as $\sigma \simeq \sqrt{|D - D_1|}$, as expected for a supercritical Hopf bifurcation, and is restored then again at D_2 with the same exponent. Also, the limit-cycle centroid

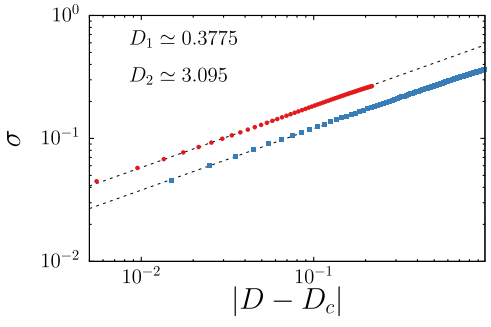

Fig. 4 Scaling behavior of the amplitude close to the bifurcation points. Dependence of the mean-field oscillation amplitude σ on $|D - D_1|$ (red circles) and $|D - D_2|$ (blue squares) where D is the diffusion value, and $D_1 \simeq 0.3775$ and $D_2 \simeq 3.095$ are the critical points corresponding to the death and restoration of the oscillations respectively. Black dashed lines correspond to power laws with exponent $\beta = 0.5$.

of each node approaches the fixed-point solution as D approaches the bifurcation point (see Supplementary Fig. 5b, c).

A supercritical Hopf bifurcation induced by the coupling is one of the main routes to Amplitude Death, the other being a saddle-node bifurcation[32]. On the other hand, OD is associated to a symmetry breaking pitchfork bifurcation, which allows for the coexistence of the oscillatory solution and the steady state[32]. Here, there is no such symmetry breaking, the inhomogeneity of the fixed point being induced by the heterogeneous coupling structure, that is not arbitrary. Moreover, the limit-cycle perishes at the bifurcation points, and thus no coexistence between the two solutions is possible. This set of observations altogether indicates that the oscillation quenching mechanism presented here falls into the category of Amplitude Death, with the novelty that the underlying fixed point is heterogeneous due to the combination of random-walk diffusion and irregular network structure. Although all the results reported so far have been obtained using the Brusselator model, in the Supplementary Note 1 we show the exact same phenomenology using the Holling-Tanner predator-prey system[43]. Additional material for the Brusselator system can be found in the Supplementary Note 2.

Sensitivity to topology and parameter modification

Network density. In order to clarify the impact that irregular network topologies have on the stabilization of the fixed point and the later restoration of the oscillations we have performed numerical simulations of the Brusselator system (10) with random-walk diffusion in different classes of complex networks (in the Supplementary Note 1 we report results corresponding the Holling-Tanner system).

As a heterogeneous network topology is key for the emergence of the amplitude death, we first consider ER networks with different average degree $\langle k \rangle$. In order to avoid fluctuations due to independent generations of the networks, that have slightly different transition points and therefore show a blurred transition when one performs an ensemble average, we choose to construct networks starting form an initial ER configuration with given size and $\langle k \rangle = 6$, and progressively add at random new connections in order to generate denser topologies with largest average degree. Figure 5a, b show the amplitude of the mean-field oscillations for different D using ER networks with increasing average degree. In Fig. 5a, we can observe that AD takes place only in sparse networks, as increasing the connectivity favors the oscillation amplitude. In Fig. 5b, the black region corresponding to AD clearly vanishes smoothly with increasing $\langle k \rangle$. In fact, for the smaller values of the average degree, oscillations are not restored even for very large values of D. As more connections are added to the topology, the stable steady state shrinks, until it completely vanishes for $\langle k \rangle \simeq 45$. The density of the connections thus is an important factor to determine the existence of AD.

Small-world network. Apart from the overall connectivity density, the inner topological structure of the network also plays a role in the AD and restoration. Indeed, for regular networks (where all nodes have the same degree), no quenching can emerge, whereas irregularity seems to induce AD. To unveil this situation, we repeat the same analysis on small-world networks generated according to the Watts-Strogatz (WS) algorithm[44] (see Methods). In this case, the network topology depends on a rewiring parameter $p \in [0, 1]$. For $p = 0$ the generated architecture corresponds to a regular network, thus homogeneous solutions exist and Turing patterns could, in principle, arise. In this case, for $p = 0$, no Turing-pattern is triggered and the fully synchronized solution is the only stable attractor. Instead, $p = 1$ corresponds to a random network similar to the ER model, and the behavior of the

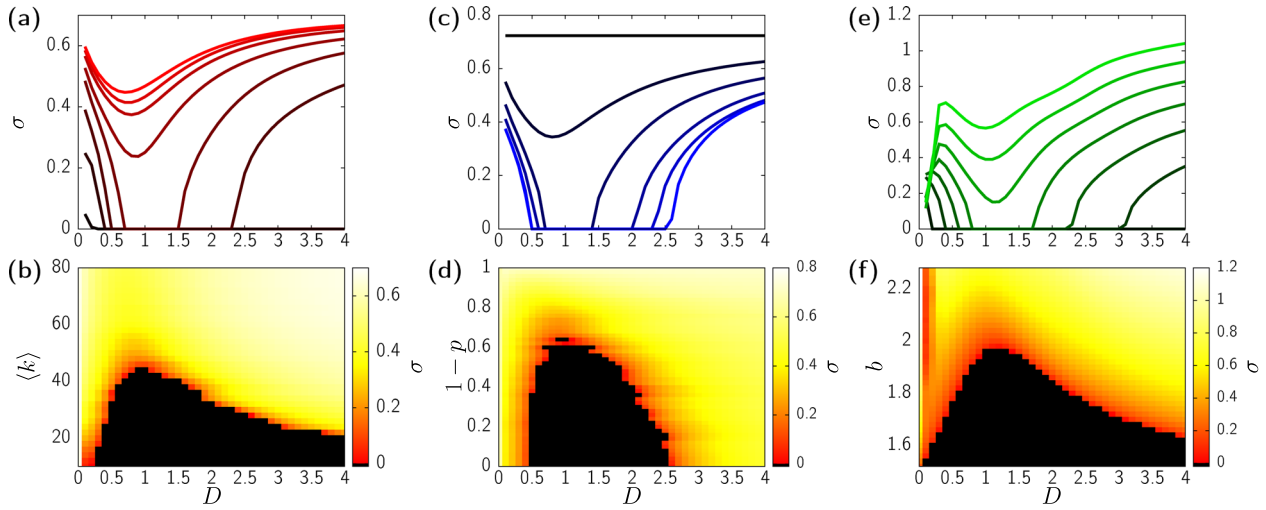

Fig. 5 Amplitude death and restoration dependence on different topological and system parameters. Top panels show the dependence of the amplitude of the mean-field oscillations on the diffusion value D. Oscillation amplitude measured as the temporal standard deviation of the y variable's mean-field, $\sigma = \sigma(\bar{y})$. Each line corresponds to a specific topological or system parameter value. Bottom panels show heatmaps of the amplitude upon tuning the diffusion and the corresponding parameter. Results obtained with simulations of the Brusselator model in networks with $N = 1000$ nodes and system parameters for the reaction terms $a = 0.5$ and $b = 1.7$ unless otherwise stated. **a**, **b** Dependence of the oscillation amplitude σ on the diffusion D in a range of Erdös-Rényi (ER) networks with different average degree $\langle k \rangle$. Values of $\langle k \rangle$ for each curve in **a** are, from top to bottom, 80, 70, 60, 50, 40, 30, 20, and 10. **c**, **d** Dependence of the oscillation amplitude σ on the diffusion D for a range of Watts-Strogatz networks with average degree $\langle k \rangle = 20$ and rewiring probability $p \in [0, 1]$. Values of $1 - p$ for each curve in **c** are, from top to bottom, 1.0, 0.8, 0.6, 0.4, 0.2, and 0. **e**, **f** Dependence of the oscillation amplitude σ on the diffusion D for different values of the system parameter b with fixed $a = 0.5$ in a single ER networks with $\langle k \rangle = 20$. Values of b for each curve in **e** are, from top to bottom, 2.2, 2.1, 2.0, 1.9, 1.8, 1.7, and 1.6.

system does not differ much from the results reported in Fig. 3a. Therefore, the behavior observed for intermediate values of p should reveal a topologically induced transition from synchronization to amplitude death.

Figure 5c, d show the outcome of such simulations in WS. As we are considering two-dimensional single-node dynamics, blue and green continuous lines show the two different branches of the dispersion relation whenever they are different, such as in panel b. networks for different values of p. To avoid fluctuations on the topology generation algorithm, we construct the networks by progressively rewiring a larger fraction of random edges in the same network. We use $1 - p$ as topological order parameter, measuring the network departure from randomness, i.e., random for $1 - p = 0$ and regular for $1 - p = 1$. As expected, for $1 - p = 0$ the situation is similar to the ER topology with $\langle k \rangle = 20$: there is a first bifurcation towards steadiness for small D, and a second bifurcation where oscillations are restored. For larger regularity, the two bifurcation points come closer together until they collide and vanish for $p \simeq 0.36$. Overall the scenario is analogous to that seen in ER networks with increasing density, but now with the disorder parameter $1 - p$ playing the role of control parameter, instead of the average degree. Both scenarios are also reminiscent of the amplitude death bifurcation observed in systems of oscillators with quenched heterogeneity[34,45]. In our case, however, the heterogeneity resides in the connectivity structure rather than in the reactive terms, which remain homogeneous.

System parameter. Finally, the choice of the dynamical parameters also plays a role on whether amplitude death arises or not. Figure 5e, f shows the outcome of numerical simulations for the same ER network with $\langle k \rangle = 20$, keeping fixed the parameter $a = 0.5$ and varying b. For $b < a + 1 = 1.5$ the reactive part does not display oscillations and the fixed point is stable. For $b > a + 1 = 1.5$ the uncoupled system undergoes a Hopf bifurcation and the stable limit-cycle emerges. Here we investigate the dynamics of the coupled system for b varying from 1.52 to 2.1. Not surprisingly, for values of b close to the bifurcation of the uncoupled system the amplitude death regime is quickly attained at small values of D, and the restoration of the oscillations is not triggered even for large coupling, i.e., the fixed point stabilizes quickly with D. As b increases, the limit-cycle has a larger amplitude and the diffusion-induced stabilization of the fixed point requires larger diffusion values. Indeed, the region of amplitude death becomes smaller as the parameter moves away from the single-node bifurcation point ($b_c = 1.5$), until it completely vanishes for $b \simeq 2.0$ in the same manner as it does when the modifications are done in the topology of the network.

Heterogeneous mean-field analysis. In order to gain some insight on the behavior of amplitude death an restoration induced by random-walk diffusion, we apply the standard tool of heterogeneous mean-field (HMF) theory[3,46], specialized to reaction–diffusion processes[18]. The basis of HMF consists in the annealed network approximation[3,47], that replaces the static adjacency matrix of a real network by an average over degree classes $\bar{a}_{ij}$ that, in the case of uncorrelated networks, takes the form

$$\bar{a}_{ij} = \frac{k_i k_j}{\langle k \rangle N} \ .$$

Introducing this expression into Eq. (2), we obtain the HMF dynamical equations

$$\begin{cases} \dot{x}_i = & f(x_i, y_i) + D(\tilde{k}_i \bar{x} - x_i) \\ \dot{y}_i = & g(x_i, y_i) + D(\tilde{k}_i \bar{y} - y_i) \end{cases} \tag{6}$$

where $\tilde{k}_i = k_i / \langle k \rangle$, $\bar{x} = \frac{1}{N} \sum_{j=1}^{N} x_j$, and $\bar{y} = \frac{1}{N} \sum_{j=1}^{N} y_j$ are the average (mean-field) activities of x and y variables. Within this framework, the dynamics of each node depends only on its own degree, the mean-field values $\bar{x}$ and $\bar{y}$, and the average connectivity of the network. In fact, one can assume then that all

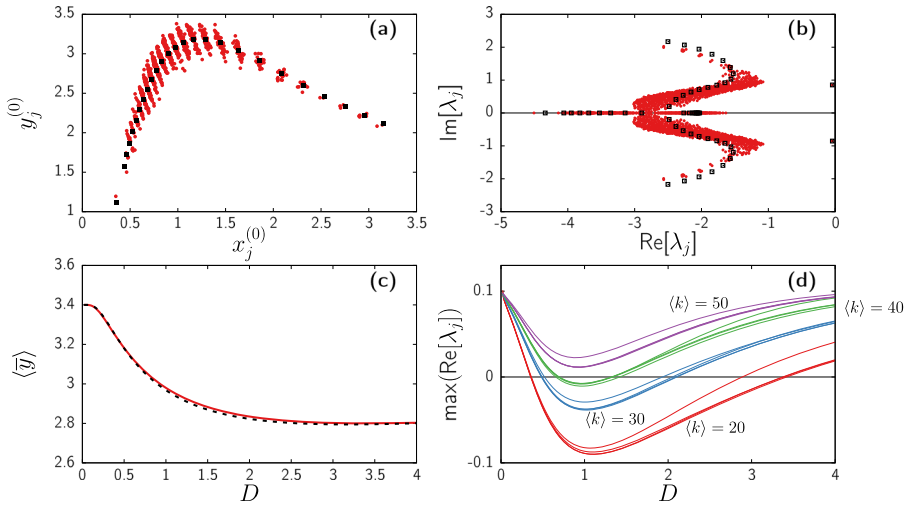

Fig. 6 Heterogeneous mean-field analysis of the Brusselator model. a Phase space for the stationary solution $(x_j^{(0)}, y_j^{(0)})$, $j = 1, ..., N$. Red circles correspond to the fixed point for diffusion value $D = 2$ as obtained from solving system (4). Black squares correspond to the mean-field result for the same D. **b** Eigenvalue spectra resulting from stability analysis. Red circles correspond to the eigenvalues λ_j, $j = 1, ..., 2N$, of the original fixed point for each for $D = 2$, whereas open black squares indicate the spectra resulting from the mean-field reduction. **c** Mean-field value of the y variable, $\bar{y}$, for the fixed point. Results obtained from directly solving system (4) (red continuous curve), and from the mean-field reduction (black dashed curve). **d** Largest eigenvalue's real part for the mean-field solution with ER networks with average degree $\langle k \rangle = 20$ (red), 30 (blue), 40 (green), and 50 (purple). For each set of networks each line denotes a different network size. From top to bottom, $N = 10^3$, 10^4, 10^5, and 10^6.

nodes with the same degree behave identically, thus formally reducing the $2N$-dimensional system (6) to a $2n$-dimensional system where n is the number of different degrees in the network[3]. An additional interest of this approach lies in the fact that it allows us to consider network sizes much larger than those permitted in a direct numerical integration, as in general $n \ll N$.

System (6) can be solved semi-analytically assuming that $\bar{x}$ and $\bar{y}$ are parameters that are to be determined self-consistently a posteriori (see Methods for details). Figure 6 shows the results of the heterogeneous mean-field approximation. In Fig. 6a, we show the fixed point obtained for the reduced system (black squares) compared with the actual fixed point obtained solving Eq. (4) (red circles) for $D = 2$. The solution of the reduced system matches the overall spreading of the solution, with the black squares fitting nicely the center of the bands displayed by the actual fixed point, corresponding to nodes with the same degree. In Fig. 6b the mean-field activity of y determined by the HFM equations (dashed black curve) matches with good accuracy that of the actual system (red continuous curve). Moreover, the stability analysis of the fixed point also coincides with that of the original system, with a cloud of eigenvalues lying far on the stable part, and a pair of complex conjugate eigenvalues crossing back and forth the imaginary axis upon modifying D. Thus, the mean-field reduction does not only provide a good proxy to study the fixed point, but also allows to study the amplitude death phenomena in terms of stability.

Large network size limit. The good agreement of the mean-field theory with the numerical results of the ER networks allows to extend our analysis to larger systems. Figure 6d shows the largest eigenvalue real part for different values of D as obtained from the heterogeneous mean-field analysis (see also the Supplementary Fig. 8). We analyzed four sets of ER networks of size $N = 10^3$, 10^4, 10^5, and 10^6, with different average degrees $\langle k \rangle = 20$, 30, 40, and 50. For a specific value of $\langle k \rangle$, we observe that networks with different sizes produce qualitatively similar results, converging to a well defined limit for sufficiently large N. For instance, for $\langle k \rangle = 20$ the upper red curve, corresponding to $N = 10^3$, shows a smaller region of amplitude death, whereas the red curves below, corresponding to larger systems, converge nicely upon increasing N. The same situation is repeated for the other values of $\langle k \rangle$, thus confirming that the effects of the average degree on the amplitude death are not finite-size but rather robust. Indeed, the overall conclusion of this analysis is that the network behavior depends strongly on the degree of each node, but is only mildly dependent on system size. In the Supplementary Figs. 4 and 7 we extend this analysis to the other topological parameters displayed in Fig. 5 for the Holling-Tanner and the Brusselator systems respectively.

Conclusion. Reaction–diffusion processes are a powerful formalism to represent general dynamical processes on networks, in which particles or species interact inside nodes while moving diffusively between pairs of connected nodes. By analogy with chemical reactions, a gradient-driven diffusion term, given by Fick's law, is usually assumed. However, in certain circumstances, a random-walk diffusion term, in which particles jump at random along edges, might be more realistic. Cases in which this kind of diffusion should be relevant include ecological dynamics, where Fick's diffusion law establishes migration only from highly populated nodes to low-concentration sites, whereas random-walk diffusion instead accounts for the well-analyzed erratic behavior of individuals[19,20]. On the other hand, in the propagation of epidemic processes, the description of the patterns of mobility and commuting of individuals is better described in terms of random-walk diffusion[5,48]. Both diffusion prescriptions are analogous in the case of homogeneous networks, but they radically differ in the presence of topological heterogeneity.

Here, we have shown how the nature of the diffusion term can alter the behavior of the limit cycles in oscillatory reaction–diffusion processes when driven by the diffusion term. Thus, although gradient–diffusion can quench the oscillations by means of an oscillation death mechanism, in which the stability of the original fixed point is preserved by the diffusion operator, random-walk diffusion generates an amplitude death quenching characterized by a inhomogeneous steady state induced by the structure of the diffusion operator. In this case, a further increase in diffusion restores the oscillations, in the form of a set of limit cycles with different amplitude for each node. The transitions to

amplitude quenching and restoration are observed to correspond to Hopf supercritical bifurcations, in agreement with an amplitude death mechanism at work. Our observations, backed up by direct numerical integration of the Brusselator systems in random networks, are confirmed by a linear stability analysis of the eigenvalues of the diffusion operator and by a seminumerical heterogeneous mean-field approximation, which allows us to check the phenomenology in very large networks. The role of random-walk diffusion in the amplitude quenching of oscillations, which is observed for different classes of homogeneous networks, different sets of parameters and even different reaction terms, is thus a robust phenomenology, which could be relevant in processes such as epidemic spreading or ecological dispersion. Future promising work along these lines would include studying the effects of a heterogeneous, scale-free topology[49], as observed in many natural networks.

Previous works on reaction–diffusion systems with random-walk diffusion focused on the emergence of inhomogeneous fixed points[5,17,18] and the study of the Turing mechanism acting on such states[17]. To our knowledge, this is the first study showing that random-walk diffusion does not only modify the steady state of the system, but it also strongly affects its stability properties beyond the Turing framework, thereby changing the macroscopic evolution of the system. In particular, this study represents an instance of diffusion-induced stabilization of a fixed point, opposed to the Turing mechanism where the steady state is destabilized through the interactions between sites. From the point of view of potential applications, our results indicate that oscillatory ecological systems could be stabilized to a steady state if the diffusion of species between patches is tuned to an appropriate interval of values, which implies that seasonal variations in the mobility of animals could result in an alternation between oscillatory and steady situations. From a more theoretical perspective, by relaxing the simplifying constrain $D_x \neq D_y$ we have imposed, it might be possible to link the amplitude death and oscillation death frameworks, by obtaining a Turing-like bifurcation pattern using random-walk diffusion. This could potentially lead to the emergence of OD in the case the oscillatory state is the one destibilized by the coupling[41]. We leave the investigation of this issue for future work.

Methods

Dispersion relation in reaction–diffusion processes. For a detailed introduction on Turing patterns and how to compute dispersion relations on regular lattices the reader can check Murray's book[39]. Here we summarize the results of Nakao et al.[7] on reaction–diffusion systems in complex networks. Let us consider a reaction–diffusion system in a complex network with a gradient-driven diffusion term

$$\begin{cases} \dot{x}_i = & f(x_i, y_i) + D_x \sum_{j=1}^{N} \Delta_{ij} x_j, \\ \dot{y}_i = & g(x_i, y_i) + D_y \sum_{j=1}^{N} \Delta_{ij} y_j, \end{cases}$$

with a Laplacian matrix $\Delta_{ij} = a_{ij} - k_i \delta_{ij}$. This Laplacian matrix is semi-definite negative, and its eigenvalues are all real and non-positive. Let $(x^{(0)}, y^{(0)})$ be a fixed point of the uncoupled system ($D_x = D_y = 0$), and hence the homogeneous solution of the coupled system. Inserting an arbitrary perturbation $\{(\delta x_i(t), \delta y_i(t))\}_{i=1}^{N}$ of the homogeneous solution to the equations and retaining up to first-order terms one gets that the evolution of the perturbation behaves as

$$\begin{pmatrix} \dot{\delta x_i} \\ \dot{\delta y_i} \end{pmatrix} = J\left(x^{(0)}, y^{(0)}\right) \begin{pmatrix} \delta x_i \\ \delta y_i \end{pmatrix} + \sum_{j=1}^{N} \Delta_{ij} \begin{pmatrix} D_x \delta x_j \\ D_y \delta y_j \end{pmatrix}, \tag{7}$$

where J is the Jacobian of the homogeneous system, evaluated at $(x^{(0)}, y^{(0)})$. Let $\Phi^{(\alpha)} = (\phi_1^{(\alpha)}, \ldots, \phi_N^{(\alpha)})^T$ be the Laplacian normalized eigenvector associated the eigenvalue Λ_α for $\alpha = 1, \ldots, N$, such that

$$\sum_m \Delta_{jm} \phi_m^{(\alpha)} = \Lambda_\alpha \phi_j^{(\alpha)}. \tag{8}$$

We can express the perturbation of the homogeneous solution in terms of the basis of the eigenvectors as

$$\begin{pmatrix} \delta x_j \\ \delta y_j \end{pmatrix} = \sum_{\alpha=1}^{N} \begin{pmatrix} u^{(\alpha)} \\ v^{(\alpha)} \end{pmatrix} \phi_j^{(\alpha)}.$$

Applying this change of coordinates on Eq. (7) and making use of the relation (8) and of the linear independence of the eigenvectors $\{\Phi^{(\alpha)}\}_{\alpha=1}^{N}$ one obtains that the evolution of $(\dot{u}^{(\alpha)}, \dot{v}^{(\alpha)})^T$ becomes independent for each $\alpha = 1, \ldots, N$ through the relation

$$\begin{aligned} \left(\dot{u}^{(\alpha)} \dot{v}^{(\alpha)}\right) &= J\left(x^{(0)}, y^{(0)}\right) \begin{pmatrix} u^{(\alpha)} \\ v^{(\alpha)} \end{pmatrix} + \Lambda_\alpha \begin{pmatrix} D_x u^{(\alpha)} \\ D_y v^{(\alpha)} \end{pmatrix} \\ &= \begin{pmatrix} \frac{\partial f}{\partial x}\left(x^{(0)}, y^{(0)}\right) + D_x \Lambda_\alpha & \frac{\partial g}{\partial x}\left(x^{(0)}, y^{(0)}\right) \\ \frac{\partial f}{\partial y}\left(x^{(0)}, y^{(0)}\right) & \frac{\partial g}{\partial y}\left(x^{(0)}, y^{(0)}\right) + D_y \Lambda_\alpha \end{pmatrix} \begin{pmatrix} u^{(\alpha)} \\ v^{(\alpha)} \end{pmatrix}. \end{aligned} \tag{9}$$

Thus, the stability of the homogeneous solution simplifies to the study of the eigenvalues (and eigenvectors) of the previous 2×2 matrix, which are obtained as functions of the Laplacian eigenvalues Λ_α. See below for an explicit application to the Brusselator system. The extension of this analysis to limit cycles makes use of Floquet theory, see[12].

The Brusselator. The Brusselator[25] is a prototypical model of autocatalytic chemical reaction with two-species showing oscillatory behavior in the form of a limit cycle. In its dimensionless form, in the absence of diffusion, it is defined by the reaction terms

$$\begin{aligned} f(x, y) &= 1 - x(b+1) + ax^2 y, \\ g(x, y) &= bx - ax^2 y, \end{aligned} \tag{10}$$

where $a, b > 0$ are model parameters. The system has a single fixed point at $(x^{(0)}, y^{(0)}) = (1, b/a)$, whose stability is ruled by the Jacobian

$$J\left(x^{(0)}, y^{(0)}\right) = \begin{pmatrix} b-1 & a \\ -b & -a \end{pmatrix}.$$

The fixed point is therefore stable for $b < a + 1$. Otherwise, the system exhibits periodic behavior, with a period, for b close to $1 + a$, approximately equal to $T = 2\pi/\sqrt{a}$. The transition from the fixed point to the oscillatory regime is through a supercritical Hopf bifurcation. Unless otherwise stated, the system parameter values used in the paper are $a = 0.5$ and $b = 1.7$.

When considering the Brusselator reaction terms (10) with Fick's diffusion (1) one can obtain the dispersion relation of the homogeneous fixed point. Following Eq. (9), one only needs to to compute the eigenvalues of

$$\begin{pmatrix} b - 1 + D_x \Lambda_\alpha & a \\ -b & -a + D_y \Lambda_\alpha \end{pmatrix},$$

which yields

$$\lambda_\pm(\Lambda_\alpha) = \frac{1}{2}\left(b - a - 1 - \Lambda_\alpha(D_x + D_y) \pm \sqrt{(D_y - D_x)\Lambda_\alpha + b - 1 + a - 4ab}\right).$$

This is the continuous curve displayed in Fig. 1a.

Dispersion of the fixed point. Let $(x_i^{(0)}(D), y_i^{(0)}(D))$ be the fixed-point solution of the reaction–diffusion system (2) with diffusion value D, so that

$$\begin{cases} f\left(x_i^{(0)}(D), y_i^{(0)}(D)\right) + D \sum_{j=1}^{N} \tilde{\Delta}_{ij} x_j^{(0)}(D) = 0 \\ g\left(x_i^{(0)}(D), y_i^{(0)}(D)\right) + D \sum_{j=1}^{N} \tilde{\Delta}_{ij} y_j^{(0)}(D) = 0. \end{cases} \tag{11}$$

for $i = 1, \ldots, N$. Assuming a smooth dependence of $(x_j^{(0)}(D), y_j^{(0)}(D))$ on D for $j = 1, \ldots, N$, we consider a small increment of the diffusion $\epsilon > 0$. The aim is to solve then

$$f\left(x_i^{(0)}(D+\epsilon), y_i^{(0)}(D+\epsilon)\right) + (D+\epsilon) \sum_{j=1}^{N} \tilde{\Delta}_{ij} x_j^{(0)}(D+\epsilon) = 0 \text{ and}$$

$$g\left(x_i^{(0)}(D+\epsilon), y_i^{(0)}(D+\epsilon)\right) + (D+\epsilon) \sum_{j=1}^{N} \tilde{\Delta}_{ij} y_j^{(0)}(D+\epsilon) = 0.$$

Expanding such equations around $(x_j^{(0)}(D), y_j^{(0)}(D))$ and retaining the first-order terms one obtains,

$$\epsilon f_x\left(x_i^{(0)}(D), y_i^{(0)}(D)\right) \frac{dx_i^{(0)}(D)}{dD} + \epsilon f_y\left(x_i^{(0)}(D), y_i^{(0)}(D)\right) \frac{dy_i^{(0)}(D)}{dD} + \epsilon \sum_{j=1}^{N} \tilde{\Delta}_{ij} \left(D \frac{dx_j^{(0)}(D)}{dD} + x_j^{(0)}(D)\right) = 0 \text{ and}$$

$$\epsilon g_x\left(x_i^{(0)}(D), y_i^{(0)}(D)\right) \frac{dx_i^{(0)}(D)}{dD} + \epsilon g_y\left(x_i^{(0)}(D), y_i^{(0)}(D)\right) \frac{dy_i^{(0)}(D)}{dD} + \epsilon \sum_{j=1}^{N} \tilde{\Delta}_{ij} \left(D \frac{dy_j^{(0)}(D)}{dD} + y_j^{(0)}(D)\right) = 0.$$

Dividing then both sides of these equations by ϵ one finally can write the differential system that rules the dependence of $(x_i^{(0)}, y_i^{(0)})$ on D,

$$J\left(x_i^{(0)}, y_i^{(0)}\right)\begin{pmatrix}\frac{dx_i^{(0)}}{dD}\\ \frac{dy_i^{(0)}}{dD}\end{pmatrix} + D\sum_{j=1}^{N}\tilde{\Delta}_{ij}\begin{pmatrix}\frac{dx_j^{(0)}}{dD}\\ \frac{dy_j^{(0)}}{dD}\end{pmatrix} = -\sum_{j=1}^{N}\tilde{\Delta}_{ij}\begin{pmatrix}x_j^{(0)}\\ y_j^{(0)}\end{pmatrix} \quad \text{for } i = 1, \ldots, N$$

where $J(x, y)$ is the 2×2 Jacobian matrix of the (uncoupled) reactive field, $(f(x, y), g(x, y))$. The previous equation is thus an implicit linear non-autonomous system of differential equations that can be solved by means of usual numerical integrators using as initial condition for $D = 0$ the solution of the uncoupled oscillators.

Network models. All networks used in this work have been generated numerically using the igraph C library[50].

ER networks. The ER model for network generation provides random network topologies[1]. In particular, we use the $G(N, p)$ model, where each pair of nodes is connected with probability $p \in [0, 1]$. The average degree of the network is then $\langle k \rangle = pN$ and the degree distribution follows a binomial distribution with parameters $N - 1$ and p.

WS model. The WS model generates networks with small-world connectivity, i.e., with small density and diameter, while still showing a large degree of transitivity or clustering[44]. We use this model as way to generate networks halfway between random and regular topologies. The model starts with N nodes distributed on a ring, each node being connected to its $\langle k \rangle$ nearest neighbors. Then, every edge of the network is rewired with probability $p \in [0, 1]$. The small-world network class is represented for small values of the rewiring probability, whereas for p close to 1 the topology becomes closer to that of a ER network.

Heterogeneous mean-field analysis. We consider the HMF equations Eq. (6) specialized for the Brusselator reaction terms. Solving for the fixed point one obtains that (dropping the subindices for simplicity), we obtain

$$y = \frac{1 - x(b+1) + D(\tilde{k}\bar{x} - x)}{-ax^2} = \frac{bx + D\bar{y}}{ax^2 + D}, \tag{12}$$

from where one can obtain a cubic equation for the value of x:

$$-a(D+1)x^3 + a(1 + D(\bar{x} + \bar{y}))x^2 - D(b + 1 + D)x + D(1 + D\bar{x}) = 0 .$$

Thus,

$$x = \frac{-1}{3a}\left(b + C + \frac{\Delta_0}{C}\right) \tag{13}$$

where,

$$C = \left(\frac{\Delta_1 \pm \sqrt{\Delta_1^2 - 4\Delta_0^3}}{2}\right)^{1/3}$$

$$\begin{aligned}\Delta_0 &= a^2(1 + D(\bar{x} + \bar{y}))^2 - 3aD(D+1)(b + 1 + D)\\ \Delta_1 &= 2a^2(1 + D(\bar{x} + \bar{y}))^2\\ &\quad - 9a^2D(D+1)(b + 1 + D)(1 + D(\bar{x} + \bar{y}))\\ &\quad + 27a^2(D+1)D(1 + D\bar{x}).\end{aligned}$$

The Brusselator system has the property that, in the fixed point and even without using any kind of approximation, $\bar{x} = 1$. However, in order to obtain $\bar{y}$ self-consistently one needs to rely on numerics. In practice, one starts with an educated guess for the mean-field $\bar{y}$ and determines then all x_j and y_j using equations (13) and (12). Using a bisection method one can reduce the error between the new estimated values $\bar{x}$ and $\bar{y}$ and the initial ones to the desired accuracy.

Data availability

Network topologies used in this study are available from the corresponding author upon reasonable request. No other data sets were generated or analyzed during the current study.

Received: 30 September 2020; Accepted: 17 December 2020;
Published online: 26 January 2021

References

1. Newman, M. *Networks: An Introduction*. (Oxford University Press, Inc., New York, NY, USA, 2010).
2. Barrat, A., Barthelemy, M. & Vespignani, A. Dynamical processes on complex networks. (Cambridge university press, 2008).
3. Dorogovtsev, S. N., Goltsev, A. V. & Mendes, J. F. F. Critical phenomena in complex networks. *Rev. Mod. Phys.* **80**, 1275–1335 (2008).
4. Hata, S., Nakao, H. & Mikhailov, A. S. Dispersal-induced destabilization of metapopulations and oscillatory turing patterns in ecological networks. *Sci. Rep.* **4**, 3585 (2014).
5. Colizza, V., Pastor-Satorras, R. & Vespignani, A. Reaction-diffusion processes and metapopulation models in heterogeneous networks. *Nat. Physics* **3**, 276–282 (2007).
6. Hanski, I. & Gaggiotti, O. Ecology, Genetics and Evolution of Metapopulations. (Elsevier Science, Princeton, 2004).
7. Nakao, H. & Mikhailov, A. S. Turing patterns in network-organized activator-inhibitor systems. *Nat. Phys.* **6**, 544–550 (2010).
8. Turing, A. M. The chemical basis of morphogenesis. *Philos. Trans. R. Soc. London B* **237**, 37–72 (1952).
9. Pecora, L. M. & Carroll, T. L. Master stability functions for synchronized coupled systems. *Phys. Rev. Lett.* **80**, 2109–2112 (1998).
10. Asllani, M., Challenger, J. D., Pavone, F. S., Sacconi, L. & Fanelli, D. The theory of pattern formation on directed networks. *Nat. Commun.* **5**, 4517 (2014).
11. Fernandes, L. D. & de Aguiar, M. A. M. Turing patterns and apparent competition in predator-prey food webs on networks. *Phys. Rev. E* **86**, 056203 (2012).
12. Challenger, J. D., Burioni, R. & Fanelli, D. Turing-like instabilities from a limit cycle. *Phys. Rev. E* **92**, 022818 (2015).
13. Petit, J., Lauwens, B., Fanelli, D. & Carletti, T. Theory of turing patterns on time varying networks. *Phys. Rev. Lett.* **119**, 148301 (2017).
14. Asllani, M., Carletti, T. & Fanelli, D. Tune the topology to create or destroy patterns. *Eur. Phys. J. B* **89**, 260 (2016).
15. Cencetti, G. et al. Topological stabilization for synchronized dynamics on networks. *Eur. Phys. J. B* **90**, 9 (2017).
16. Cencetti, G., Clusella, P. & Fanelli, D. Pattern invariance for reaction-diffusion systems on complex networks. *Sci. Rep.* **8**, 16226 (2018).
17. Angstmann, C. N., Donnelly, I. C. & Henry, B. I. Pattern formation on networks with reactions: a continuous-time random-walk approach. *Phys. Rev. E* **87**, 032804 (2013).
18. Baronchelli, A., Catanzaro, M. & Pastor-Satorras, R. Bosonic reaction-diffusion processes on scale-free networks. *Phys. Rev. E* **78**, 016111 (2008).
19. Turchin, P. Quantitative Analysis of Movement: Measuring and Modeling Population Redistribution in Animals and Plants. Weimar and Now; 13. https://books.google.es/books?id=ZbdmQgAACAAJ (Sinauer, 1998).
20. Okubo, A. & Levin, S. *Diffusion and Ecological Problems: Modern Perspectives. Interdisciplinary Applied Mathematics*. https://books.google.es/books?id=tU7UBwAAQBAJ (Springer New York, 2013).
21. Masuda, N., Porter, M. A. & Lambiotte, R. Random walks and diffusion on networks. *Phys. Rep.* **716-717**, 1–58 (2017).
22. Cencetti, G., Battiston, F., Fanelli, D. & Latora, V. Reactive random walkers on complex networks. *Phys. Rev. E* **98**, 052302 (2018).
23. Asslani, M., Di Patti, F. & Fanelli, D. Stochastic turing patterns on a network. *Phys. Rev. E* **86**, 046105 (2012).
24. Kuramoto, Y. *Chemical Oscillations, Waves and Turbulence* (Springer, Berlin, 1984).
25. Prigogine, I. & Lefever, R. Symmetry breaking instabilities in dissipative systems. ii. *J. Chem. Phys.* **48**, 1695–1700 (1968).
26. Guevara, M., Glass, L. & Shrier, A. Phase locking, period-doubling bifurcations, and irregular dynamics in periodically stimulated cardiac cells. *Science* **214**, 1350–1353 (1981).
27. Michaels, D. C., Matyas, E. P. & Jalife, J. Mechanisms of sinoatrial pacemaker synchronization: a new hypothesis. *Circ. Res.* **61**, 704–714 (1987).
28. Buzsaki, G. *Rhythms of the Brain*. https://books.google.es/books?id=7rFuVK3MkzIC (Oxford University Press, 2006).
29. Izhikevich, E. M. & Edelman, G. M. Large-scale model of mammalian thalamocortical systems. *Proc. Natl. Acad. Sci.* **105**, 3593–3598 (2008).
30. Freund, J. A., Mieruch, S., Scholze, B., Wiltshire, K. & Feudel, U. Bloom dynamics in a seasonally forced phytoplankton–zooplankton model: Trigger mechanisms and timing effects. *Ecol. Complex.* **3**, 129–139 (2006).
31. Baurmann, M., Gross, T. & Feudel, U. Instabilities in spatially extended predator–prey systems: spatio-temporal patterns in the neighborhood of turing–hopf bifurcations. *J. Theor. Biol.* **245**, 220–229 (2007).
32. Koseska, A., Volkov, E. & Kurths, J. Oscillation quenching mechanisms: amplitude vs. oscillation death. *Phys. Rep.* **531**, 173–199 (2013).
33. Aronson, D., Ermentrout, G. & Kopell, N. Amplitude response of coupled oscillators. *Phys. D Nonlinear Phenomena* **41**, 403–449 (1990).
34. Mirollo, R. E. & Strogatz, S. H. Amplitude death in an array of limit-cycle oscillators. *J. Stat. Phys.* **60**, 245–262 (1990).
35. Ramana Reddy, D. V., Sen, A. & Johnston, G. L. Time delay induced death in coupled limit cycle oscillators. *Phys. Rev. Lett.* **80**, 5109–5112 (1998).
36. Konishi, K. Amplitude death induced by dynamic coupling. *Phys. Rev. E* **68**, 067202 (2003).

37. Samukhin, A. N., Dorogovtsev, S. N. & Mendes, J. F. F. Laplacian spectra of, and random walks on, complex networks: are scale-free architectures really important? *Phys. Rev. E* **77**, 036115 (2008).
38. Strogatz, S. Nonlinear Dynamics and Chaos: With Applications to Physics, Biology, Chemistry, and Engineering. https://books.google.es/books?id=1kpnDwAAQBAJ (CRC Press, 2018).
39. Murray, J. Mathematical Biology II: Spatial Models and Biomedical Applications. Interdisciplinary Applied Mathematics. https://books.google.es/books?id=s2QKBwAAQBAJ (Springer New York, 2006).
40. Asllani, M., Carletti, T., Fanelli, D. & Maini, P. K. A universal route to pattern formation in multicellular systems. *Eur. Phys. J. B* **93**, 135 (2020).
41. Koseska, A., Volkov, E. & Kurths, J. Transition from amplitude to oscillation death via turing bifurcation. *Phys. Rev. Lett.* **111**, 024103 (2013).
42. Galassi, M. & Gough, B. GNU Scientific Library: Reference Manual. https://books.google.es/books?id=EkeAQgAACAAJ (Network Theory, 2003).
43. Tanner, J. T. The stability and the intrinsic growth rates of prey and predator populations. *Ecology* **56**, 855–867 (1975).
44. Watts, D. J. & Strogatz, S. H. Collective dynamics of 'small-world' networks. *Nature* **393**, 440–442 (1998).
45. Saxena, G., Prasad, A. & Ramaswamy, R. Amplitude death: the emergence of stationarity in coupled nonlinear systems. *Physics Reports* **521**, 205–228 (2012).
46. Pastor-Satorras, R. & Vespignani, A. Epidemic spreading in scale-free networks. *Phys. Rev. Lett.* **86**, 3200–3203 (2001).
47. Boguñá, M., Castellano, C. & Pastor-Satorras, R. Langevin approach for the dynamics of the contact process on annealed scale-free networks. *Phys. Rev. E* **79**, 036110 (2009).
48. Balcan, D. et al. Multiscale mobility networks and the spatial spreading of infectious diseases. *Proc. Natl. Acad. Sci.* **106**, 21484–21489 (2009).
49. Barabási, A.-L. & Albert, R. Emergence of scaling in random networks. *Science* **286**, 509–512 (1999).
50. Csardi, G. & Nepusz, T. The igraph software package for complex network research. *J. Complex Syst.* **1695**, 1–9 (2006).

Acknowledgements

We acknowledge financial support from the Spanish MINECO, under projects no. FIS2016-76830-C2-1-P and no. FIS2016-76830-C2-2-P, and Spanish MICINN, under Projects no. PID2019-106290GB-C21 and no. PID2019-106290GB-C22. R.P.-S. acknowledges additional financial support from ICREA Academia, funded by the Generalitat de Catalunya.

Author contributions

R.P.-S. and M.-C.M. designed the research. P.C. developed the theoretical analysis. All authors analyzed the results and wrote the paper.

Competing interests

The authors declare no competing interests.

Additional information

Supplementary information is available for this paper at https://doi.org/10.1038/s42005-020-00516-w.

Correspondence and requests for materials should be addressed to P.C.

Reprints and permission information is available at http://www.nature.com/reprints

Publisher's note Springer Nature remains neutral with regard to jurisdictional claims in published maps and institutional affiliations.